(and even more at lower sulfate concentrations). Although some of the methane would have been reoxidized in the sediment by anaerobic methane oxidation coupled to sulfate reduction (*27*), considerable methane would have escaped (*28*) and could have substantially contributed to the greenhouse warming of the early Earth (*3*, *4*).

Sediment-supported rates of sulfate reduction are highly sensitive to sulfate concentrations from 100 to 1000 μM (Fig. 2B), and the isotope record (*2*, *6*) indicates that sulfate concentrations increased beyond 200 μM starting around 2.4 Ga. The concomitant increase in sulfate reduction rate, both in sediments and in the water column as sulfate became more available, would have reduced methanogenesis substantially, as well as the flux of methane to the atmosphere. This, in concert with a possible rise in atmospheric O_2 providing an increased methane sink, may have led to global cooling and the first known glaciation at around 2.4 Ga (*4*).

References and Notes

1. H. D. Holland, *The Chemical Evolution of the Atmosphere and Oceans* (Princeton Univ. Press, Princeton, NJ, 1984).
2. D. E. Canfield, K. S. Habicht, B. Thamdrup, *Science* **288**, 658 (2000).
3. A. A. Pavlov, J. F. Kasting, L. L. Brown, K. A. Rages, R. Freedman, *J. Geophys. Res.* **105**, 11981 (2000).
4. J. F. Kasting, A. A. Pavlov, J. L. Siefert, *Origins Life Evol. Biosphere* **31**, 271 (2001).
5. A. G. Harrison, H. G. Thode, *Trans. Faraday Soc.* **53**, 84 (1958).
6. D. E. Canfield, in *Stable Isotope Geochemistry*, J. W. Valley, D. R. Cole, Eds. (Mineralogical Society of America, Blacksburg, VA, 2001), vol. 43, pp. 607–636.
7. K. Ingvorsen, B. B. Jørgensen, *Arch. Microbiol.* **139**, 61 (1984).
8. K. Ingvorsen, A. J. B. Zehnder, B. B. Jørgensen, *Appl. Environ. Microbiol.* **27**, 1029 (1984).
9. H. Cypionka, in *Sulfate-Reducing Bacteria*, L. L. Barton, Ed. (Plenum, New York, 1995), pp. 151–184.
10. A. N. Roychoudhury, E. Viollier, P. Van Cappellen, *Appl. Geochem.* **13**, 269 (1998).
11. Materials and methods are available as supporting material on *Science* Online.
12. B. B. Jørgensen, *Geochim. Cosmochim. Acta* **43**, 363 (1979).
13. T. Kagegawa, H. Ohmoto, *Precam. Res.* **96**, 209 (1999).
14. H. Ohmoto, T. Kakegawa, D. R. Lowe, *Science* **262**, 555 (1993).
15. T. Kagegawa, Y. Kasahara, K.-I. Hayashi, H. Ohmoto, *Geochem. J.* **34**, 121 (2000).
16. Y. Shen, R. Buick, D. E. Canfield, *Nature* **410**, 77 (2001).
17. Some of the basins from before 2.7 Ga, for which sulfur isotope values are available, may have experienced sulfate concentrations different from those of the global ocean. Lower sulfate concentrations may have been possible if the basin experienced restricted exchange with the ocean, and higher concentrations could have been possible if local sulfate sources were available. The lack of high fractionations, except where high-sulfate environments can be documented (*16*), implies that throughout the wide range of depositional conditions sampled [see data in (*2*)], sulfate concentrations before 2.7 Ga were low. We must conclude that low sulfate concentrations were a persistent feature of marine depositional environments, and we furthermore emphasize that variability in sulfate concentrations within the global ocean was likely.
18. J. Farquhar, H. M. Bao, M. Thiemens, *Science* **289**, 756 (2000).
19. J. Farquhar, J. Savarino, S. Airieau, M. H. Thiemens, *J. Geophys. Res. Planets* **106**, 32829 (2001)
20. R. E. Stoiber, S. N. Williams, B. Huebert, *J. Volcanol. Geotherm. Res.* **33**, 1 (1987).
21. W. T. Holser, M. Schidlowski, F. T. Mackenzie, J. B. Maynard, in *Chemical Cycles in the Evolution of the Earth*, C. B. Gregor, R. M. Garrels, F. T. Mackenzie, J. B. Maynard, Eds. (Wiley, New York, 1988), pp. 105–173.
22. J. C. M. de Hoog, B. E. Taylor, M. J. van Bergen, *Earth Planet. Sci. Lett.* **189**, 237 (2001).
23. E. K. Berner, R. A. Berner, *Global Environment: Water, Air, and Geochemical Cycles* (Prentice-Hall, Upper Saddle River, NJ, 1996).
24. J. C. G. Walker, P. Brimblecombe, *Precam. Res.* **28**, 205 (1985)
25. M. Holmer, P. Storkholm, *Freshwater Biol.* **46**, 431 (2001).
26. K. S. Habicht, M. Gade, B. Thamdrup, P. Berg, D. E. Canfield, data not shown.
27. W. S. Reeburgh, *Earth Planet. Sci. Lett.* **28**, 337 (1976).
28. C. S. Martens, J. V. Klump, *Geochim. Cosmochim. Acta* **44**, 471 (1980).
29. J. J. Middelburg, K. Soetaert, P. M. J. Herman, *Deep-Sea Res.* **44**, 327 (1997).

30. We thank C. Bjerrum for discussions, two reviewers for helpful comments, and L. Salling and P. Søholt for expert assistance in the lab. The project was funded by the Danish National Research foundation (Grundforskningsfond) and the Danish Research Council (SNF).

Supporting Online Material

www.sciencemag.org/cgi/content/full/298/5602/2372/DC1
Materials and Methods
Fig. S1
References

9 September 2002; accepted 13 November 2002

Interannual Variability in the North Atlantic Ocean Carbon Sink

Nicolas Gruber,[1]* Charles D. Keeling,[2] Nicholas R. Bates[3]

The North Atlantic is believed to represent the largest ocean sink for atmospheric carbon dioxide in the Northern Hemisphere, yet little is known about its temporal variability. We report an 18-year time series of upper-ocean inorganic carbon observations from the northwestern subtropical North Atlantic near Bermuda that indicates substantial variability in this sink. We deduce that the carbon variability at this site is largely driven by variations in winter mixed-layer depths and by sea surface temperature anomalies. Because these variations tend to occur in a basinwide coordinated pattern associated with the North Atlantic Oscillation, it is plausible that the entire North Atlantic Ocean may vary in concert, resulting in a variability of the strength of the North Atlantic carbon sink of about ±0.3 petagrams of carbon per year (1 petagram = 10^{15} grams) or nearly ±50%. This extrapolation is supported by basin-wide estimates from atmospheric carbon dioxide inversions.

The ocean's contribution to the observed interannual variability of atmospheric carbon dioxide (CO_2) is poorly established. Estimates based on atmospheric measurements of CO_2, oxygen, and stable carbon isotopes indicate that the variability contributed by the oceanic carbon cycle is more than ±1 Pg C $year^{-1}$ (*1*–*4*). In contrast, estimates based on direct observations of the partial pressure of CO_2 (pCO_2) in surface waters (*5*, *6*) and on modeling studies (*7*, *8*) indicate a contribution of less than ±0.5 Pg C $year^{-1}$, mainly associated with tropical Pacific ocean variability caused by El Niño and La Niña (*9*). However, many uncertainties are associated with the modeling studies, and the equatorial Pacific is the only region where interannual variability in oceanic pCO_2 has been directly observed and documented. Given evidence for substantial extratropical variability in sea surface temperature (SST) (*10*) and the ocean's state (*11*), other oceanic regions may contribute substantially to the atmospheric CO_2 variability as well. The North Atlantic Ocean is one of the few regions where enough data are available to investigate interannual to decadal variability in the extratropical ocean carbon cycle. Observationally based estimates (*12*), as well as forward and inverse modeling results (*13*), indicate that this region constitutes the largest ocean sink for atmospheric CO_2 in the Northern Hemisphere, on average taking up about 0.7 ± 0.1 Pg C $year^{-1}$.

Observations have shown that most of the interannual to decadal climatic variability in the North Atlantic basin occurs in broadly coherent patterns linked to a natural mode of atmospheric pressure variation known as the North Atlantic Oscillation (NAO) (*14*). The

[1]Institute of Geophysics and Planetary Physics and Department of Atmospheric Sciences, University of California, Los Angeles, CA 90095, USA. [2]Scripps Institution of Oceanography, University of California, San Diego, La Jolla, CA 92093, USA. [3]Bermuda Biological Station for Research, Inc., Ferry Reach GE01, Bermuda.

*To whom correspondence should be addressed. E-mail: ngruber@igpp.ucla.edu

NAO is a large-scale seesaw in atmospheric mass between a subtropical high-pressure system, typically near the Azores, and a subpolar low near Iceland (*15*). In the Atlantic Ocean, a positive phase of the NAO, i.e., a stronger pressure gradient between these two systems, is expressed by positive SST anomalies in the subtropics and the marginal seas of northern Europe and negative anomalies in the subpolar gyres (*16*, *17*). These anomalies are accompanied by changes in oceanic convection, in which regions of warmer SSTs experience less vigorous winter mixing than normal, whereas regions of cold SSTs experience deeper winter mixing (*18*).

We examined interannual variability in the carbon cycle of the upper layers of the North Atlantic Ocean, and its connection with the NAO, on the basis of an 18-year time series of dissolved inorganic carbon (DIC), total alkalinity (Alk), and the $^{13}C/^{12}C$ ratio of DIC obtained from near-surface waters at two stations near Bermuda (*19*) (Fig. 1). The Bermuda time series shows distinct seasonal oscillations for salinity-normalized DIC (sDIC), its $^{13}C/^{12}C$ ratio [expressed as $\delta^{13}C$ (*20*)], and computed pCO_2 (*21*), but it exhibits only occasional short-term changes in salinity-normalized Alk (sAlk) (Fig. 1A). sDIC, $\delta^{13}C$, and pCO_2 show distinct long-term trends related to the uptake of isotopically depleted anthropogenic CO_2 from the atmosphere (*22*–*24*). The observed long-term rate of increase of sDIC over the period from October 1983 to June 2001 is 0.64 ± 0.05 μmol kg^{-1} $year^{-1}$ (*25*). The corresponding rate of increase for pCO_2 is found to be 1.5 ± 0.1 parts per million (ppm) $year^{-1}$, very close to the observed atmospheric trend over the same period and consistent with the expectation that subtropical near-surface waters mix too slowly with deeper waters to be substantially displaced from equilibrium with anthropogenically perturbed atmospheric CO_2. The long-term decrease in $\delta^{13}C$ is -0.024 ± 0.001 per mil $year^{-1}$, close to the trends observed previously in subtropical regions (*23*, *26*).

To highlight interannual variability, we removed the mean seasonal cycle and the long-term trend by subtracting a linear trend and harmonics with 12-, 6-, and 4-month periods from the data. The resulting anomalies revealed significant interannual variability in sDIC and in its isotopic ratio $\delta^{13}C$ that are well correlated with anomalies in SST and winter mixed-layer depth (Fig. 1B and table S1). By contrast, the corresponding variability of pCO_2 was relatively low, amounting to only a few ppm. This low variability was a consequence of compensating effects between anticorrelated interannual SST and sDIC anomalies (*24*). Nevertheless, the forcing of pCO_2 by SST anomalies is stronger than by the sDIC anomalies, as previously noted with regard to the seasonal cycle (*27*), which leads to a positive correlation between pCO_2 and SST anomalies (table S1). SST and mixed-layer depth anomalies near Bermuda have been shown to be significantly correlated with the NAO (*24*, *28*),

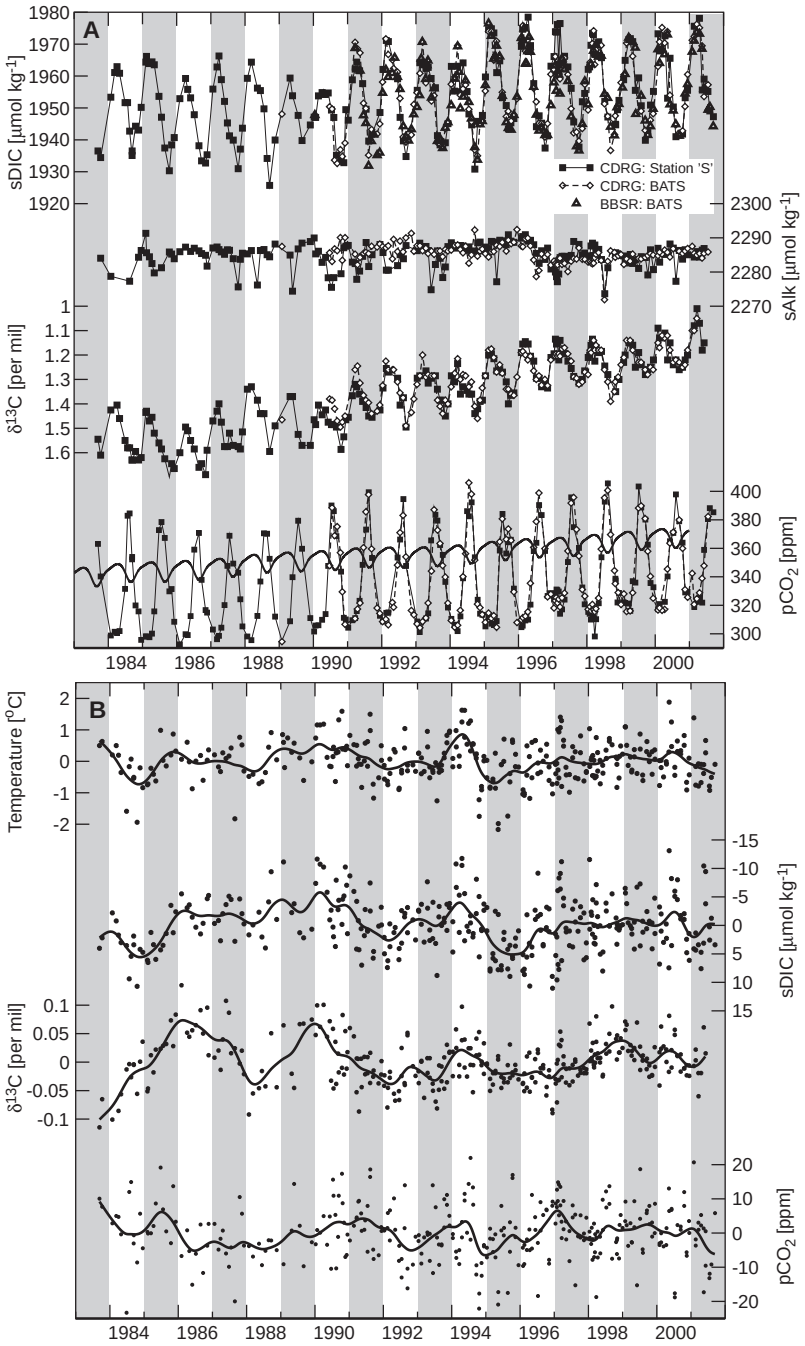

Fig. 1. Time series of properties in the upper-ocean mixed layer of the northwestern Sargasso Sea near Bermuda (Station S at 32°10′N, 64°30′W and the BATS site at 31°50′N, 64°10′W). (**A**) Observations of inorganic carbon. The reduced isotopic $^{13}C/^{12}C$ ratio of DIC, $\delta^{13}C$, is shown inverted to make the seasonal and long-term relation with DIC more evident. The concentrations of DIC and Alk (sDIC and sAlk) have been normalized to a constant salinity of 35. pCO_2 has been computed from DIC, Alk, SST, and sea-surface salinity and is compared with the partial pressure of atmospheric CO_2. The latter has been calculated with the mean atmospheric pressure and humidity observed at St. Davids Head on the island of Bermuda and observations of the atmospheric CO_2 mixing ratio [with data from La Jolla, CA (*1*), for 1982 to 1995 and from Bermuda (*46*) for 1989 to 2000]. Data labeled CDRG (squares and diamonds) were analyzed at the Scripps Institution of Oceanography; data labeled BBSR (triangles) were measured at Bermuda Biological Station for Research. (**B**) Seasonally adjusted and long-term linearly detrended time series of SST, $\delta^{13}C$, sDIC, and pCO_2. Smoothing splines (cut-off period of 1 year) have been added to emphasize trends. The sDIC anomalies have been inverted to emphasize the interannual correlation with temperature anomalies ($\delta^{13}C$ is not inverted).

with warmer-than-normal conditions and reduced wintertime mixing during positive phases of the NAO. Our analysis of the 1983 to 2001 data is consistent with these previous analyses. A division of the correlation analysis into three periods (December through March, April through July, and August through November) shows that the strongest correlations are found in winter, when the NAO pattern is most strongly expressed in the atmosphere (*14*).

We also found a strong correlation of the NAO with sDIC anomalies. In contrast, the correlations for $\delta^{13}C$ and pCO_2 were weak. Both results agree with the findings of Bates (*24*), who analyzed the Bermuda Biological Station for Research (BBSR) record for the Bermuda Atlantic Timeseries Study (BATS) from 1988 to 1998.

Our aim was to elucidate quantitatively the processes that influence the surface oceanic carbon cycle (such as air-sea gas exchange, biology, mixing, and transport) and to determine how these processes interact to cause the observed correlations. To this end, we used a simple diagnostic box model of the upper-ocean carbon cycle (*29*) that exploits the previous finding that the dominant control of seasonal variations in $\delta^{13}C$ in near-surface water DIC is net community production (*30*). We combined an estimate of the isotopic fractionation associated with net community production with estimates of air-sea gas exchange, vertical entrainment, and vertical diffusion, which permitted us to estimate the magnitude and variability of net community production and horizontal transport, the only two processes that cannot be estimated on the basis of simple parameterizations (*31*).

The mean seasonal fluxes for the 1983 to 2001 period derived from this diagnostic approach are very similar to those found for the 1991 to 1994 period (*29*), which indicates relatively stable seasonal behavior. These results demonstrate that the seasonal dynamics of mixed-layer DIC near Bermuda is dominated by the net removal of DIC in the spring and summer as a result of net community production. This biologically induced drawdown of DIC is aided in summer by the outgassing of CO_2 due to the winter-to-summer warming of the surface ocean. The seasonal cycle is closed by vertical entrainment and uptake of CO_2 from the atmosphere in fall and winter. Vertical diffusion plays a minor role, whereas our calculations indicate a small addition of DIC throughout the year as a result of horizontal transport processes. The magnitude and sign of this inferred horizontal transport are consistent with estimates computed from the horizontal DIC gradient and from the observed horizontal velocities (*32*). Summarized over the annual cycle, the carbon balance in the mixed layer is established between the net removal of carbon by net community production (3.4 ± 0.8 mol m^{-2} $year^{-1}$) (*33*), the net addition of carbon by gas exchange (1.9 ± 0.2 mol m^{-2} $year^{-1}$), entrainment (1.6 ± 0.4 mol m^{-2} $year^{-1}$), diffusion (0.6 ± 0.3 mol m^{-2} $year^{-1}$), and horizontal transport (1.3 ± 0.4 mol m^{-2} $year^{-1}$). The flux budget is closed by a "rectifier" flux term that arises because of the strong covariance of mixed-layer depth and DIC (*31*).

Interannual variability strongly modifies these annual mean fluxes with variations up to $\pm 50\%$ from their mean values (Fig. 2). These variations strongly correlate with mixed-layer depth variability and SST anomalies (Fig. 2 and table S1) and suggest that these latter two parameters represent key processes controlling interannual variability near Bermuda. Because DIC increases with depth, the flux of inorganic carbon into the mixed layer is increased during winters with deeper convection. As a consequence, a positive DIC anomaly is generated in conjunction with anomalously cool SSTs, which are caused by increased heat loss at the surface and by cooling induced by mixing with deeper waters (*16*). Our model calculations indicate that these years of cool water tend to have up to 0.8 mol m^{-2} $year^{-1}$ higher-than-average uptake of CO_2 from the atmosphere, a joint result of negative pCO_2 anomalies caused by the cooler-than-normal SSTs and of the stronger-than-normal winds. The contribution from horizontal transport also tends to be enhanced but to a significantly smaller degree. Finally, annual net community production is up to 1 mol m^{-2} $year^{-1}$ higher than average, a finding corroborated by concurrently observed increases in net primary productivity (*24*). These results are consistent with the argument that, in nutrient-limited systems such as that found near Bermuda, the increase in the entrainment of nutrients should lead to enhanced biological productivity (*34*).

Figure 3 summarizes the findings of our analysis of interannual variability of the carbon cycle near Bermuda by contrasting a year with shallow winter mixing and warm SST anomalies with a year with opposite characteristics. The positive DIC anomalies and negative $\delta^{13}C$ anomalies, accompanying a cooler-than-average year, are primarily caused by the increased vertical supply of waters from the thermocline, which is high in DIC and low in $\delta^{13}C$, and increased uptake of isotopically light CO_2 from the atmosphere. The magnitudes of these anomalies are reduced by an increase in net community production that removes isotopically light carbon from the near-surface ocean water. However, this compensation is incomplete,

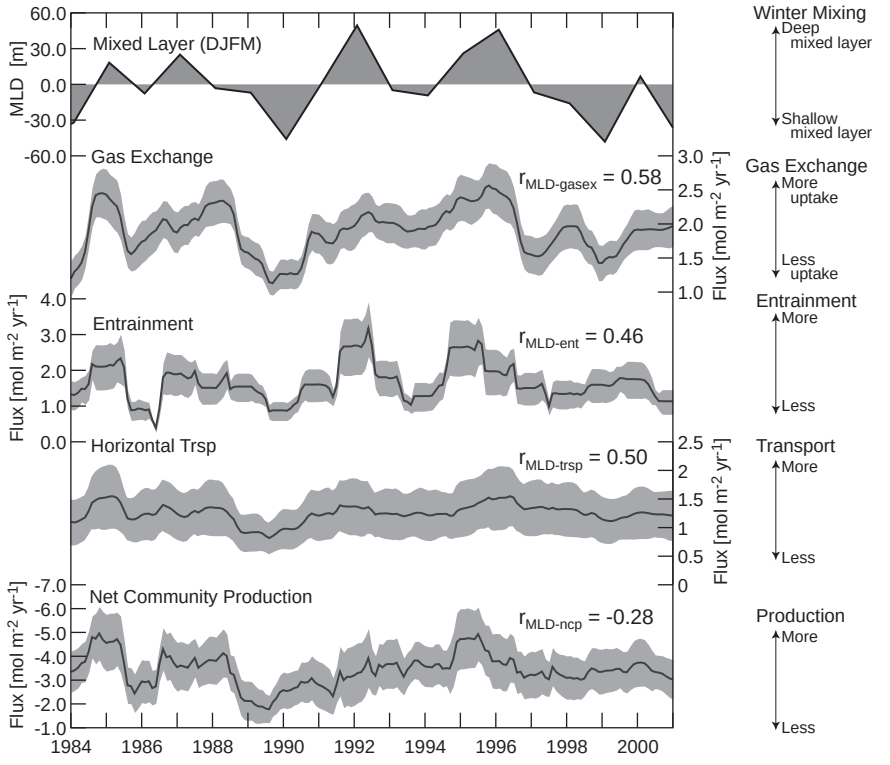

Fig. 2. Twelve-month running mean fluxes of CO_2 gas exchange, entrainment, horizontal transport, and net community production as computed by our diagnostic model. All processes are significantly correlated with mixed-layer anomalies shown in the top panel (correlation coefficients, *r*, are shown on the right), with years of deeper mixed layers tending to have higher uptake of CO_2 from the atmosphere, higher entrainment fluxes, increased horizontal transport, and elevated net community production. The shading indicates a 1-σ uncertainty interval determined from Monte Carlo simulations. DJFM, December through March; MLD, mixed-layer depth; trsp, transport.

leading to a positive DIC anomaly, which persists for the entire year. During warmer-than-normal years, the opposite is the case, with net community production compensating less than normal. This interaction between mixed-layer depth variability, air-sea gas exchange, and biological activity not only leads to the generation of DIC and $\delta^{13}C$ anomalies but also affects the magnitude of the seasonal cycle. Years of cool water and deep winter mixing tend to show large seasonal cycles, because all processes are acting vigorously; years of warm water and shallow mixing typically show a reduced seasonal cycle.

Anomalies in mixing and SST near Bermuda during winter tend to extend over the entire western subtropical gyre (*16*, *35*) and are linked to the NAO (*17*). Given the importance of mixing and temperature variability in driving interannual variability in the carbon cycle near Bermuda, we would expect that this cycle varies in a concerted manner with Bermuda over the entire subtropical gyre. This might most likely be the case for air-sea gas exchange, which showed a high and significant correlation with the NAO near Bermuda (table S1). If the amplitude of the air-sea CO_2 flux anomaly observed near Bermuda ($\pm$0.8 mol m^{-2} year^{-1}) is representative of the entire gyre, the subtropical North Atlantic carbon sink (15°N to 40°N) has varied by up to $\pm$0.2 Pg C year^{-1} since 1983, enough to contribute measurably to Northern Hemisphere–scale atmospheric CO_2 anomalies. We unfortunately lack long-term time-series observations of pCO_2 at other places in the North Atlantic subtropical gyre with which to assess our extrapolation. Some supporting evidence comes from deeper ocean DIC observations made at BATS from 1988 to the present (*36*), which revealed substantial DIC variability in subtropical mode waters. Bates *et al.* (*36*) show that these variations most likely reflect NAO-related variations in the net uptake of CO_2 from the atmosphere in the regions where these subtropical mode waters are formed, thus representing a record of past variations in air-sea CO_2 fluxes in the regions several hundred kilometers north of Bermuda.

Further support for our extrapolation is provided by an inverse modeling analysis of atmospheric CO_2 variations (*37*), which showed a pattern of anomalous CO_2 flux for the entire North Atlantic consistent in phasing and magnitude with our Bermuda results (Fig. 4). This suggests that possibly the entire North Atlantic might vary in concert with Bermuda. If we scale the air-sea CO_2 flux anomalies from the Bermuda site to the entire North Atlantic, this oceanic sink for atmospheric CO_2 may vary on the order of $\pm$0.3 Pg C year^{-1}, or nearly $\pm$50% of its mean strength.

Although the air-sea CO_2 flux anomalies estimated from our long-term record near Bermuda are consistent with atmospheric CO_2 inversions, the lack of direct oceanic observations, and the uncertainties associated with atmospheric inversion analysis, make these extrapolations tentative. Time-series observations of the subpolar gyre of the North Atlantic are required to confirm our estimates and to clarify the response of the extratropical carbon cycle to interannual variations in meteorological forcing (*8*). Understanding the climate sensitivity of the oceanic carbon cycle on these shorter time scales is imperative if we are to predict how the oceanic carbon cycle will respond to future climatic change.

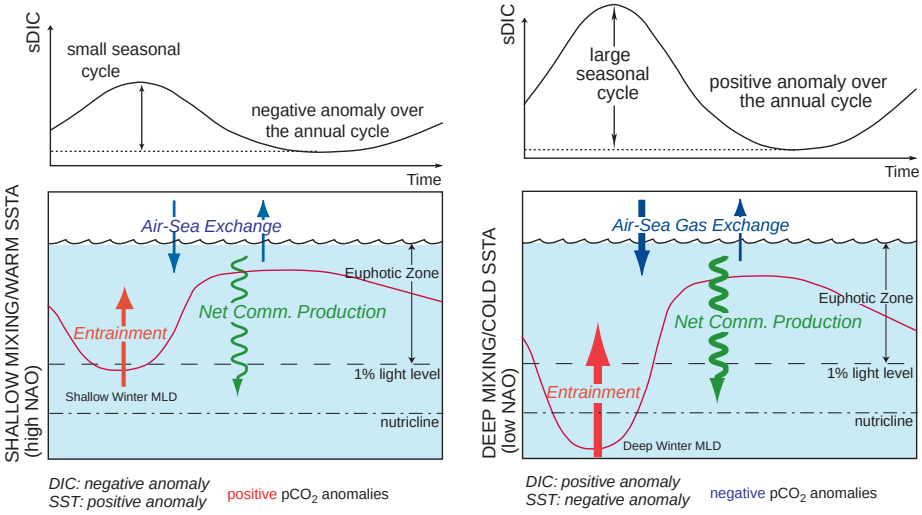

Fig. 3. Schematic depiction of the seasonal carbon cycle near Bermuda, modified in response to interannual variations in mixed-layer depth and SST. In warmer-than-normal years that have shallow winter mixed layers (a typically positive NAO index), little DIC and few nutrients are brought into the upper ocean, which promotes less net community production than normal. In addition, the uptake of CO_2 from the atmosphere is reduced because of positive SST anomalies and reduced wind speeds. As a result, the seasonal cycle of sDIC is suppressed. In contrast, colder years exhibit deeper mixed layers with larger entrainment, enhanced net community productivity, and higher CO_2 uptake from the atmosphere, which produces an enhanced seasonal cycle of sDIC. SSTA, SST anomalies.

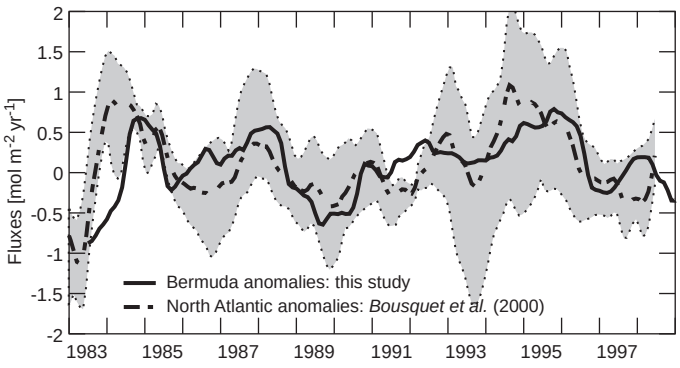

Fig. 4. Comparison of the air-sea CO_2 flux anomalies estimated for Bermuda from direct observations (solid line) with the air-sea CO_2 flux anomalies estimated with an inverse model applied to the entire North Atlantic region (broken line) (*37*). The model estimate of flux (mol m^{-2} year^{-1}) is derived from an inversion of atmospheric CO_2 data yielding an integrated flux, which then was divided by the area of the North Atlantic between 20°N and 80°N (30×10^{12} m^2). The broken line represents the mean result of eight atmospheric inversions; gray shading indicates the range of results. The air-sea flux anomalies at Bermuda have been smoothed with a 1-year running average filter.

References and Notes

1. C. D. Keeling, T. P. Whorf, M. Wahlen, J. van der Plicht, *Nature* **375**, 666 (1995).
2. R. J. Francey *et al.*, *Nature* **373**, 326 (1995).
3. M. Battle *et al.*, *Science* **287**, 2467 (2000).
4. P. Bousquet *et al.*, *Science* **290**, 1342 (2000).
5. R. A. Feely, R. Wanninkhof, T. Takahashi, P. Tans, *Nature* **398**, 597 (1999).
6. K. Lee, R. Wanninkhof, T. Takahashi, S. C. Doney, R. A. Feely, *Nature* **396**, 155 (1998).
7. A. M. E. Winguth *et al.*, *Global Biogeochem. Cycles* **8**, 39 (1994).
8. C. LeQuéré, J. C. Orr, P. Monfray, O. Aumont, G. Madec, *Global Biogeochem. Cycles* **14**, 1247 (2000).
9. F. P. Chavez *et al.*, *Science* **286**, 2126 (1999).
10. R. Kawamura, *J. Phys. Oceanogr.* **24**, 707 (1994).
11. D. Stammer *et al.*, *J. Geophys. Res.* **107**, 3118 (2002), 10.1029/200/JC000888.
12. T. Takahashi *et al.*, *Deep Sea Res. II* **49**, 1601 (2002).
13. M. Gloor *et al.*, *Geophys. Res. Lett.*, in press.
14. J. W. Hurrell, *Science* **269**, 676 (1995).
15. J. Bjerknes, *Adv. Geophys.* **10**, 1 (1964).
16. D. R. Cayan, *J. Phys. Oceanogr.* **22**, 859 (1992).
17. H. M. Cullen, R. D. D'Arrigo, E. R. Cook, M. E. Mann, *Paleoceanography* **16**, 27 (2001).
18. R. Dickson, J. Lazier, J. Meincke, P. Rhines, J. Swift, *Progr. Oceanogr.* **38**, 241 (1996).
19. In 1983, the Carbon Dioxide Research Group (CDRG) of the Scripps Institution of Oceanography started a program to collect and analyze near-surface ocean

samples (from 2- and 10-m depth) for DIC, Alk, and $\delta^{13}C$ at Station S, located 26 km southeast of the island of Bermuda (32°10′N, 64°30′W) (*27*). In 1989, the Joint Global Ocean Flux Study BATS program was established at a station 56 km further southeast (31°50′N, 64°10′W) (*38*). The CDRG program extended their measurements to this new site, and the BBSR started to measure DIC there throughout the water column (*24*). Because differences between Station S and BATS have been found to be small (*38*), and because the DIC data from the two laboratories show no systematic differences (change in DIC = -1.0 ± 2.2 μmol kg^{-1}, $N = 78$ measurements), the data from the two sites and two laboratories are combined here into a single time series.

20. The reduced isotopic ratio, $\delta^{13}C$, is defined as $\delta^{13}C = ({}^{13}r_{sample} - {}^{13}r_{std})/{}^{13}r_{std}$, where ${}^{13}r_{sample}$ is the $^{13}C/^{12}C$ ratio of the sample, and where ${}^{13}r_{std}$ is the $^{13}C/^{12}C$ ratio of the Pee Dee belemnite standard.
21. We computed the oceanic pCO_2 from the observed temperature, salinity, Alk, DIC, and nutrients using a thermodynamic model of the carbonate system (*39*) and the dissociation constants of Mehrbach *et al*. (*40*) as refitted by Dickson and Millero (*41*). This choice is based on laboratory studies (*42*) and the resulting good agreement with direct observations of pCO_2 near Bermuda (*43*).
22. R. B. Bacastow, C. D. Keeling, T. J. Lueker, M. Wahlen, W. G. Mook, *Global Biogeochem. Cycles* **10**, 335 (1996).
23. N. Gruber *et al.*, *Global Biogeochem. Cycles* **13**, 307 (1999).
24. N. R. Bates, *Deep-Sea Res. II* **48**, 1507 (2001).
25. This trend is smaller than that reported by Bates (*24*) for 1988 to 1998, mainly because of smaller growth rates in the 1980s.
26. R. E. Sonnerup *et al.*, *Global Biogeochem. Cycles* **13**, 857 (1999).
27. C. D. Keeling, in *The Global Carbon Cycle*, M. Heimann, Ed. (Springer-Verlag, New York, 1993), pp. 413–430.
28. T. M. Joyce, P. Robbins, *J. Clim.* **9**, 3121 (1996).
29. N. Gruber, C. D. Keeling, T. F. Stocker, *Deep-Sea Res. I* **45**, 673 (1998).
30. Net community production refers to the net transfer between inorganic and organic carbon pools due to photosynthesis and to oxidation of organic matter, and therefore is equal to net primary production minus community respiration.
31. Materials and methods are available as supporting material on *Science* Online.
32. Because the time-series sites are located in the broad recirculation region of the subtropical North Atlantic, the geostrophic mean currents are from the northeast. Current meter data indicate a mean current of about 0.05 m s^{-1} (*44*), although substantially higher velocities are associated with the passage of eddies. Based on the observed mean horizontal gradient near Bermuda of about 1.1×10^{-5} μmol kg^{-1} m^{-1} (*29*), our model-derived transport estimates give horizontal velocities of between −0.01 and −0.20 m s^{-1}, with a long-term mean of −0.07 m s^{-1} (negative velocity indicates southward flow).
33. The uncertainties of the fluxes have been established with a Monte Carlo technique (*45*). The diagnostic model was run 1000 times, with randomly selected sets of parameter values within a predetermined range for each parameter based on the parameter's perceived uncertainty (*29*). The flux uncertainties listed in the text denote the 1-σ uncertainty computed from the results of these 1000 realizations.
34. Because our diagnostic model analyses cannot uniquely determine the underlying mechanisms, other factors, such as variations in mesoscale eddy dynamics, or dust deposition and its possible impact on N_2 fixation, could be responsible for our positive correlation of net community production with winter mixed-layer depth anomalies.
35. R. L. Molinari, D. A. Mayer, J. F. Festa, H. F. Bezdek, *J. Geophys. Res.* **102**, 3267 (1997).
36. N. R. Bates, A. C. Pequignet, R. J. Johnson, N. Gruber, *Nature* **420**, 489 (2002).
37. The atmospheric CO_2 inversion results have been provided by P. Bousquet and P. Peylin and are based on the anomalous CO_2 fluxes for the entire North Atlantic region as estimated in their global study (*4*).
38. A. F. Michaels, A. H. Knap, *Deep-Sea Res. II* **43**, 157 (1996).
39. U.S. Department of Energy, "Handbook of methods for the analysis of the various parameters of the carbon dioxide system in sea water," version 2, *Tech. Rep. ORNL/CDIAC-74* (U.S. Department of Energy, Carbon Dioxide Information Analysis Center, Oak Ridge National Laboratory, Oak Ridge, TN, 1994).
40. C. Mehrbach, C. H. Culberson, J. E. Hawley, R. M. Pytkowicz, *Limnol. Oceanogr.* **18**, 897 (1973).
41. A. G. Dickson, F. J. Millero, *Deep-Sea Res.* **34**, 1733 (1987).
42. T. J. Lueker, A. G. Dickson, C. D. Keeling, *Mar. Chem.* **70**, 105 (2000).
43. N. R. Bates, T. Takahashi, D. W. Chipman, A. H. Knap, *J. Geophys. Res.* **103**, 15567 (1998).
44. D. A. Siegel, W. G. Deuser, *Deep-Sea Res. I* **44**, 1519 (1997).
45. R. Y. Rubinstein, *Simulation and the Monte Carlo Method* (Wiley, New York, 1981).
46. T. J. Conway *et al.*, *J. Geophys. Res.* **99**, 22831 (1994).
47. We are grateful to the numerous people who have been responsible for the collection, preparation, and analysis of the data presented here. We thank in particular P. Guenther, T. Lueker, G. Emanuele, E. Bollenbacher, and A. Dickson at the Scripps Institution of Oceanography. We also thank A. Knap, A. Michaels, D. Steinberg, C. Carlson, and D. Hansell for their help and support. We are grateful to P. Bousquet and P. Peylin for providing us with their atmospheric CO_2 inversion results for the North Atlantic. Supported by NSF grants OCE-0097337 (N.G.) and OCE-0083918 (C.D.K.) and by grants from the NSF and NOAA (N.R.B.).

Supporting Online Material

www.sciencemag.org/cgi/content/full/298/5602/2374/DC1
Materials and Methods
Table S1
References and Notes

7 August 2002; accepted 13 November 2002

Control of Facial Muscle Development by MyoR and Capsulin

Jian-rong Lu,[1] Rhonda Bassel-Duby,[1] April Hawkins,[1] Priscilla Chang,[1] Renee Valdez,[1] Hai Wu,[1] Lin Gan,[4] John M. Shelton,[2] James A. Richardson,[1,3] Eric N. Olson[1]*

Members of the MyoD family of basic helix-loop-helix (bHLH) transcription factors control the formation of all skeletal muscles in vertebrates, but little is known of the molecules or mechanisms that confer unique identities to different types of skeletal muscles. MyoR and capsulin are related bHLH transcription factors expressed in specific facial muscle precursors. We show that specific facial muscles are missing in mice lacking both *MyoR* and *capsulin*, reflecting the absence of MyoD family gene expression and ablation of the corresponding myogenic lineages. These findings identify *MyoR* and *capsulin* as unique transcription factors for the development of specific head muscles.

The myogenic bHLH transcription factors—MyoD, Myf5, myogenin, and MRF4—control vertebrate skeletal muscle development (*1*). *MyoD* and *Myf5* act redundantly as myoblast specification genes (*2*), whereas *myogenin* is required for myoblast differentiation (*3*, *4*). *MyoD* and *MRF4* also play redundant roles in muscle differentiation (*5*). Although these myogenic genes control a developmental program shared by all skeletal muscles, there is evidence that muscles in the head and trunk differ with respect to the early steps in myogenic lineage specification (*6*). For example, in *Myf5*$^{-/-}$*Pax-3*$^{-/-}$ double-mutant mice, the trunk musculature is eliminated, but head muscles are unaffected (*7*). The developmental control genes responsible for head muscle formation are unknown.

All skeletal muscle posterior to the head is derived from paraxial mesoderm that becomes segmented into somites (*1*, *8*). In contrast, head muscles are derived from multiple cell lineages, including prechordal mesoderm anterior to the first somite and paraxial mesodermal precursors that migrate into the branchial arches (*9*–*11*). MyoR/musculin and capsulin/Pod-1/epicardin are related bHLH proteins transiently expressed in migratory paraxial mesodermal cells in the branchial arches that appear to represent precursors of the muscles of mastication (*12*–*18*).

A null mutation in the mouse *capsulin* gene results in neonatal lethality due to pulmonary hypoplasia, but no overt skeletal muscle abnormalities (*18*, *19*). We combined mutations in *MyoR* and *capsulin* to see if there were shared activities or effects not revealed with either single-gene deletion. The *MyoR* gene was targeted in embryonic stem (ES) cells by homologous recombination (fig. S1A). ES cell clones

[1]Department of Molecular Biology, [2]Department of Internal Medicine, and [3]Department of Pathology, The University of Texas Southwestern Medical Center at Dallas, 6000 Harry Hines Boulevard, Dallas, TX 75390–9148, USA. [4]Center for Aging and Developmental Biology, University of Rochester, Rochester, NY 14642, USA

*To whom correspondence should be addressed. E-mail: eolson@hamon.swmed.edu